Atmospheric Research 276 (2022) 106270

Contents lists available at ScienceDirect

Atmospheric Research

journal homepage: www.elsevier.com/locate/atmosres

Influence of water vapor influx on interdecadal change in summer precipitation over the source area of the Yellow River Basin

Xiaoqian Huang, Xiaodan Guan *, Kaiwei Zhu, Tonghui Gu, Jianping Huang, Yongli He

Collaborative Innovation Center for Western Ecological Safety, College of Atmospheric Sciences, Lanzhou University, Lanzhou, China

ARTICLE INFO

Keywords:
Precipitation
Moisture source
The source area of the Yellow River Basin
Interdecadal change

ABSTRACT

The source area of the Yellow River Basin (SYRB) is located in the northeastern Tibetan Plateau, and the precipitation in the SYRB is of great importance to the water resources throughout the whole basin. By analyzing the summer precipitation in the SYRB, we found that an 11.4% increase in precipitation occurred during 2003–2019 compared with 1982–2002. Such interdecadal increase of summer precipitation was due to significant changes of moisture contribution from external moisture source. In the past 38 years, 95.4% of the water vapor for summer precipitable water in the SYRB came from local evapotranspiration (10.6%), the Tibetan Plateau area (35.8%), central Eurasian area (22.5%), South Asia-northern Indian Ocean area (14.6%), South China Sea-western Pacific area (6.6%), and North Africa-West Asia area (5.3%). Thus, external water vapor supplied about 84.8% of summer precipitable water in the SYRB. Compared with 1990–2002, the relative growth rates of moisture contribution during 2003–2019 from the central Eurasian area, North Africa-West Asia area and South China Sea-western Pacific area increased by 2.40%, 4.55% and 15.07%, respectively. Such interdecadal changes were verified by evapotranspiration minus precipitation for it can illustrate the supply capacity of the moisture source. Water vapor supplies in these areas increased during 2003–2019, which greatly contributed to the increase of summer precipitation in the SYRB.

1. Introduction

The Yellow River, located in northern China, is one of the largest rivers in the world. It has been the mother river of China since ancient times (Lin et al., 2001). The Yellow River Basin (YRB) covers an area of 795,000 km^2 and extends eastward through arid, semi-arid and semi-humid regions (Hassan et al., 2008; Li et al., 2019; Yao et al., 2020). The basin supports more than 114 million people with drinking water and irrigation, which accounts for 9% of the total population, 16.2% of arable land and more than 50 cities in China (Wang et al., 2021). The source area of the Yellow River Basin (SYRB; it is our study area, which is part of the YRB over the Tibetan Plateau as the Fig. 1 shows), as the major runoff-producing and water-holding region of the Yellow River (Gao et al., 2016; Lan et al., 2010), provides 49.2% of the total runoff (Feng et al., 2006). Based on previous studies, precipitation is the major source of local water resources in the SYRB (Hu et al., 2011; Wang et al., 2006). It is important for local water replenishment, and is one of the indicators for rational development and utilization of water resources in the YRB. Decreased precipitation in the YRB led to an increased area of degraded vegetation, from 24.5% in the 1980s to 34.5% in the 1990s (Wang et al., 2001), and caused dry-off events nearly every year in the 1990s due to global warming (Liang et al., 2010; Wu et al., 2020). Accordingly, it is urgent to study the variation in precipitation in the SYRB and its mechanism. This understanding will help cope with the water resource shortage problem under climate change.

Precipitation in the SYRB has significant spatial and temporal variability, caused by diverse topography and climate change (Yuan et al., 2015; Zhang et al., 2015). Fig. 1 shows that the annual precipitation in the SYRB decreases from the southeast (approximately 800 mm) to the northwest (approximately 200 mm). However, the uneven precipitation distribution diminished during the last 50 years because the precipitation over the southeastern SYRB decreased and that over the northwestern SYRB increased (Huang et al., 2020; Li et al., 2016). From the perspective of regional average, the annual precipitation in the whole SYRB showed an upward trend after 1990 (Jiang et al., 2019; Yuan et al., 2020). The precipitation variation in the SYRB is a wide concern for the public, and some studies have discussed its causes (Yuan et al., 2015; Yuan et al., 2016; Zhang et al., 2015). At the interdecadal time scale,

* Corresponding author.
E-mail address: guanxd@lzu.edu.cn (X. Guan).

https://doi.org/10.1016/j.atmosres.2022.106270
Received 22 January 2022; Received in revised form 25 May 2022; Accepted 25 May 2022
Available online 30 May 2022

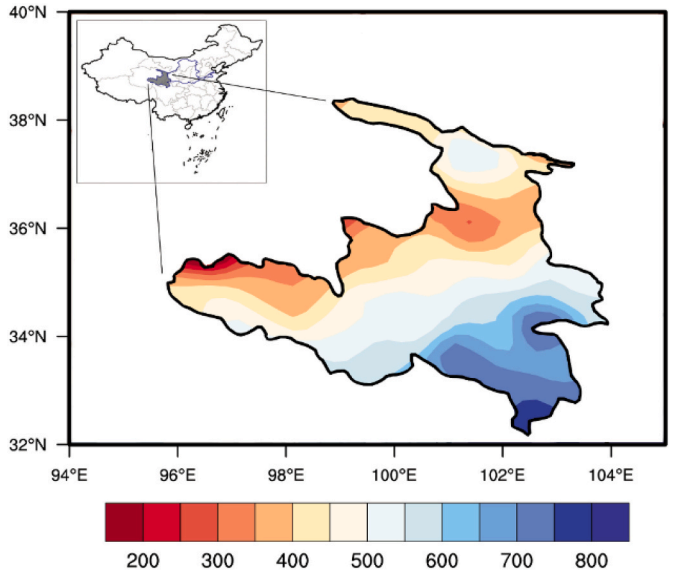

Fig. 1. Location of the source area of the Yellow River Basin, and spatial distribution of its annual precipitation (units: mm). (For interpretation of the references to colour in this figure legend, the reader is referred to the web version of this article.)

precipitation is often dominated by local water vapor changes; and these changes are usually caused by water vapor influxes (Camberlin, 1997; Lin et al., 2018; Trenberth et al., 2010; Wang and Chen, 2012). Therefore, identifying the moisture source and water vapor pathways is important for studying precipitation change. However, previous studies that addressed water vapor transport were based on conventional Eulerian grids (Guan et al., 2021; Ma et al., 2018). This method can describe water vapor pathways, but cannot assess changes in water vapor transport due to the fast transition of the wind field (Peng et al., 2020). Therefore, the moisture contribution of moisture sources is often overestimated or underestimated. To date, the accurate amount of water vapor supply and the details of transport processes for the precipitation variation in the SYRB remain unclear.

In this paper, we use the dynamic precipitation recycling model (DRM; Dominguez et al., 2006) and moisture source attribution method to identify the moisture sources and quantify the moisture contribution to summer precipitable water in the SYRB. Both qualitative and quantitative methods are used here to illustrate the mechanism of precipitation change. The rest of this paper is organized as follows. In Section 2, we introduce the datasets, DRM and moisture source attribution method used in this study. In Section 3, we present the main results, including the change in summer precipitation, moisture sources and the mechanism of summer precipitation change during 1982–2019. In Section 4, summary and discussion are given.

2. Methodology and data

2.1. Methodology

2.1.1. Water vapor budget calculation

To evaluate the impact of water vapor influxes on precipitation over the SYRB, we calculate water vapor content and vertically integrated horizontal water vapor flux by using

$$\mathrm{WV} = -\frac{1}{g}\int_{300hPa}^{p_s} qdp \tag{1}$$

$$Q_u = -\frac{1}{g}\int_{300hPa}^{p_s} qudp \tag{2}$$

$$Q_v = -\frac{1}{g}\int_{300hPa}^{p_s} qvdp \tag{3}$$

where WV is water vapor content; Q_u and u represent zonal water vapor flux and wind, respectively; Q_v and v are the meridional water vapor flux and wind, respectively; and q, p, p_s, and g represent specific humidity, pressure, surface pressure, and gravity, respectively.

We selected a rectangular area of 96°E-104°E, 32°N–38°N, which covers the whole SYRB, to study water vapor transport across each boundary of the SYRB. Following Sun et al. (2011), the vertically integrated horizontal water vapor budget is calculated by fluxes.

At southern and northern boundaries:

$$Q_{S/N} = \int_{\lambda_W}^{\lambda_E} Q_{\varphi_{S/N}} a\cos\varphi_S d\lambda \tag{4}$$

and at western and eastern boundaries:

$$Q_{W/E} = \int_{\varphi_S}^{\varphi_N} Q_{\lambda_{W/E}} a d\varphi \tag{5}$$

where $Q_{S/N}$ and $Q_{W/E}$ are the water vapor fluxes of the southern/northern and western/eastern boundaries, respectively. Positive value indicates that water vapor is transported from west to east in latitude and from south to north in longitude, and vice versa. λ_E and λ_W are the longitudes of the eastern and western boundaries, respectively; and φ_N and φ_S are the latitudes of the northern and southern boundaries, respectively. $Q_{\varphi S/N}$ and $Q_{\lambda W/E}$ are the meridional water vapor flux of the southern/northern boundary and zonal water vapor flux of the western/eastern boundary, respectively. a is the mean radius of the Earth (6.37×10^6 m).

2.1.2. Dynamic precipitation recycling model

The DRM used in this paper provides the summer precipitation recycling ratio in the SYRB and the backward trajectory of water vapor. This model is based on the conservation of atmospheric water vapor mass equation. When we ignore liquid and ice forms of water in the atmosphere, the water vapor budget in a unit atmospheric column (Stohl and James, 2004; Trenberth, 1991) can be written as follows:

$$\frac{\partial W}{\partial t} + \nabla \bullet Q = E - P + res \tag{6}$$

where W, Q, E, and P are the precipitable water, water vapor flux, evapotranspiration, and precipitation, respectively; and res is the residual term.

Based on the following assumptions, the moisture of local evapotranspiration and advected water vapor in the atmosphere column are well mixed. Eq. (6) was vertically integrated to calculate the recycling ratio (He et al., 2021), which is derived as:

$$\frac{\partial \rho}{\partial t} + \vec{V}_{WV} \bullet \nabla\rho = \frac{(1-\rho)E}{W} \tag{7}$$

where ρ and $\vec{\mathrm{V}}_{\mathrm{WV}}$ represent the recycling ratio and water vapor velocity, respectively.

After a series of formula derivations, the precipitation recycling ratio of grid cell i of area $\Delta \mathrm{A_i}$ is calculated by using

$$\rho_i = 1 - exp\left[-\int_{s_0}^{s}\left(\frac{E}{W}\right)ds\right] \tag{8}$$

where s_0 is the original point of the moisture backward trajectory.

Finally, the local precipitation recycling ratio of the study area within N grid cells is:

$$\rho = \frac{P_M}{P} = \frac{\sum_{i=1}^{N}\rho_i P_i \Delta A_i}{\sum_{i=1}^{N} P_i \Delta A_i} \tag{9}$$

where P_M is the precipitation generated by water vapor from the study area. The DRM can be used on an hourly time scale because it includes the moisture storage term. Moreover, it is simple and computationally efficient, which has been widely used in studies on water cycle (Bisselink and Dolman, 2008; Hua et al., 2017).

2.1.3. Moisture source attribution method

The moisture source attribution method (Sodemann et al., 2008) is used to identify moisture sources for summer precipitable water in the SYRB and quantify their contributions. The water vapor influxes can be seen as an air parcel carrying moisture from a source to the SYRB along a trajectory. Because it undergoes multiple processes of absorbing and releasing moisture by evapotranspiration and precipitation, the amount of moisture in the air parcel will change over time. This method considers the processes involved, quantifying the contributions of the regions along the backward trajectory to the SYRB in the Lagrangian framework. The moisture source attribution method presented in Sodemann et al. (2008) is a three-dimensional tracking method. Here, we modify this method because the DRM is a two-dimensional model (Ren et al., 2021).

Using the DRM results, we identify the backward trajectories of water vapor, and use W to calculate the variation in water vapor. Because the retention time of water vapor in the atmosphere is approximately 10 days, we calculate the change in W along the 10-day water vapor trajectory using $\Delta W = W(t) - W(t-6\,\mathrm{h})$. The time interval is 6 h and the duration is from $t = -240$ h to $t = 0$ h in this study. A region with $\Delta W > 0$ is regarded as a moisture source, and $\Delta W < 0$ is a moisture sink. For each water vapor trajectory, the point where $\Delta W > 0$ is recorded for the first time is defined as the starting point for the trajectory. The fractional contribution (f_n) of ΔW_n to the moisture in a unit area air column (W_n) at moment n is shown as follows:

$$f_n = \frac{\Delta W_n}{W_n} \tag{10}$$

When water vapor moves toward the SYRB, in regions where $\Delta W > 0$, the increased water vapor is supplied by evapotranspiration, reducing the contribution of previous water vapor. The fractional contribution of the amount of water vapor at previous time (m) with respect to new moisture in a unit area air column at moment n is recalculated as follows:

$$f_m = \frac{\Delta W_m}{W_n}, \mathrm{m} < \mathrm{n} \tag{11}$$

And where $\Delta W < 0$, the decreased water vapor due to precipitation also reduces the contribution of previous water vapor. The water vapor change is reduced in proportion to precipitation:

$$\Delta W_m^{'} = \Delta W_m + \Delta W_n \bullet f_m, \text{for all m} < \mathrm{n} \tag{12}$$

When the water vapor reaches the SYRB, the sum of the latest fractional contributions of all uptake points constitutes the total contribution of all points on the trajectory during the entire period. One trajectory can determine some moisture sources, and the contribution of moisture sources to precipitable water is determined by the sum of all trajectories (Peng et al., 2020). Finally, the contribution percentage of the j^{th} moisture source region ($\mathrm{CP_j}$) to summer precipitable water in the SYRB is calculated as follows:

$$CP_j = \frac{\sum_{k=1}^{ktot} \Delta W^k(j)}{\sum_{k=1}^{ktot} W_{t=-6h}} \times 100\% \tag{13}$$

where k is the k^{th} water vapor trajectory.

2.2. Data

Both monthly datasets and hourly datasets used in this study cover the period from 1982 to 2019. Monthly precipitation data with a resolution of 0.25° × 0.25° is obtained from the Global Precipitation Climatology Centre (GPCC), which is based on data products from approximately 85,000 observation stations. The dense station network makes it suitable for estimating inland precipitation, such as that in the SYRB (Schneider et al., 2014; Zhu et al., 2021).

Monthly meridional and zonal water vapor fluxes are integrated from the surface to 300 hPa using specific humidity, meridional and zonal wind components at eight standard pressure levels (1000–300 hPa) and surface pressure. The variables are provided by the National Center for Environmental Prediction/National Center for Atmospheric Research (NCEP/NCAR) reanalysis dataset (Kalnay et al., 1996), which have a resolution of 2.5° × 2.5°. This dataset is widely used in studying water vapor transport and atmospheric circulation in Asia (Huang et al., 2015).

Hourly variables are used in the DRM and moisture source attribution method to identify moisture sources, including meridional and zonal winds, specific humidity at each standard pressure level (1000–300 hPa), precipitation, evapotranspiration, and total column water. All of them are from the European Centre for Medium-Range Weather Forecasts (ECMWF) reanalysis (ERA5) dataset, which has a resolution of 0.25° × 0.25°. Monthly evapotranspiration and precipitation with the same spatial resolution are also obtained from the ECMWF ERA5, which are used to analyze the water budget change in moisture sources (Zhao et al., 2021).

3. Results

Fig. 2a shows the annual cycle of precipitation in the SYRB during 1979–2019. The maximum precipitation occurred in July; and there was a significant difference in precipitation amount between summer and the other seasons. The mean summer precipitation was 278.1 mm during 1982–2019, which accounted for 55.3% of the mean annual precipitation (502.9 mm). The fluctuation in summer precipitation evolved highly in step with annual precipitation, which is revealed by the correlation coefficient up to 0.88 at the 0.01 confidence level (Fig. 2b). We will focus on summer precipitation in the rest of the paper to illustrate its moisture sources in a more rigorous way.

The summer precipitation over the SYRB has an obvious interdecadal increase from 2002 (Fig. 3a); the mean summer precipitation was 264.6 mm during 1982–2002 and 294.8 mm during 2003–2019. It shows the precipitation increased by approximately 11.4% (more than 30-mm) from the first period to the second period. The water vapor content over the SYRB and the water vapor influxes also increased by 0.85 kg m^{-2} and 1.05×10^{13} kg during 2003–2019 compared with 1982–2002 (Fig. 3b). It suggests that the interdecadal change of summer precipitation in the SYRB may be greatly influenced by water vapor influxes. Furthermore, the summer precipitation during 1982–2019 was significantly correlated with the water vapor content in the SYRB ($r = 0.73$, $p < 0.01$), and the water vapor content is positively correlated with the water vapor influxes in the whole period ($r = 0.84$, $p < 0.01$; Fig. 3b). Therefore, the summer precipitation in the SYRB is closely related with water vapor influxes. The external water vapor supply change is the cause of interdecadal increase of summer precipitation from 2002 in the study area.

Fig. 4 shows that the water vapor from the Arabian Sea and Bay of Bengal into the SYRB through southwestern China during 1982–2019. The water vapor along this path is often related to the southwesterly monsoon (Mrudula, 2016; Zhang, 2001), which brings plentiful water vapor to the SYRB in summer. The westerly wind also brings some water vapor to support summer precipitation (Fig. 4). To further understand the influence of external water vapor supply variability to water vapor content in SYRB, we analyzed the impact of the water vapor transport from the SYRB's four boundaries on water vapor content over the SYRB in summer during 1982–2019. In the meridional direction, the net water vapor transport of the southern and northern boundaries is significantly

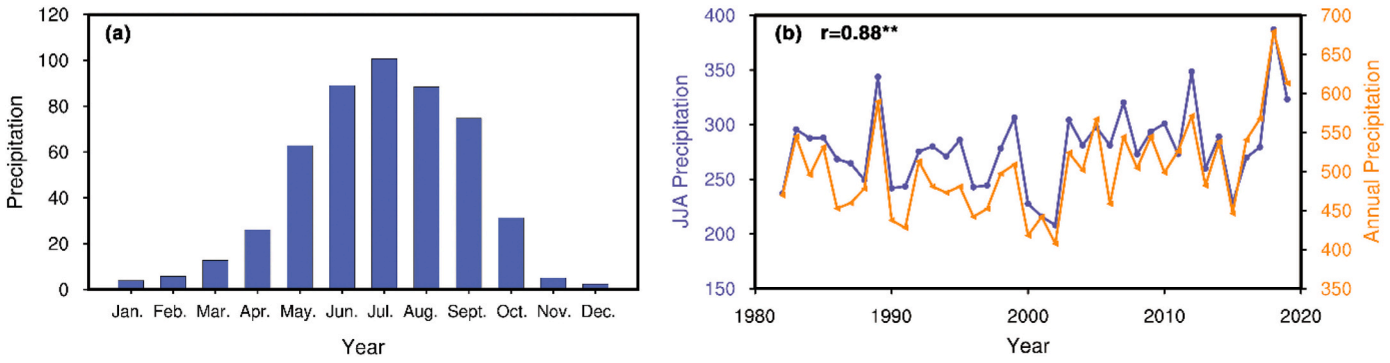

Fig. 2. (a) Monthly mean precipitation in the SYRB during 1979–2019 (units: mm). (b) The time series of annual precipitation (orange line) and summer precipitation (blue line) in the SYRB during 1979–2019 (units: mm). The correlation coefficient of annual precipitation and summer precipitation is 0.88, which passes 0.01 confidence level based on Student's *t*-test. (For interpretation of the references to colour in this figure legend, the reader is referred to the web version of this article.)

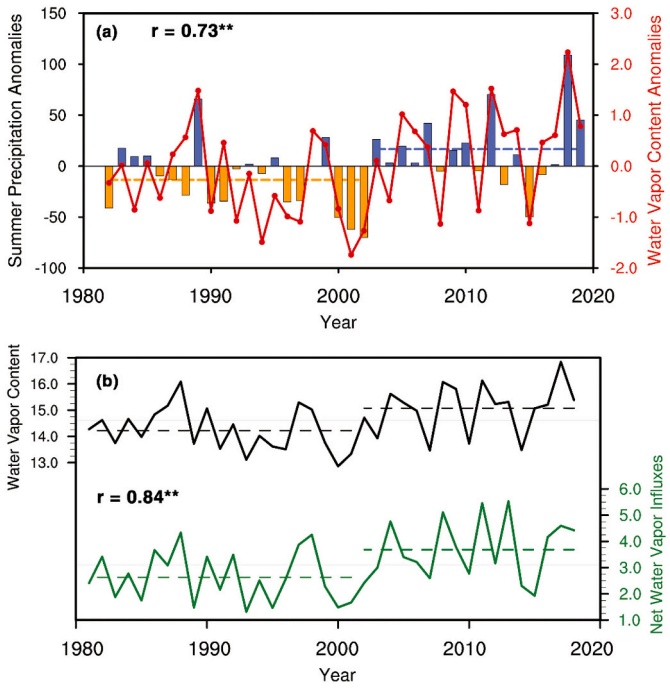

Fig. 3. (a) Time series of summer precipitation anomalies (colour bar; units: mm) and water vapor content anomalies (red solid line; units: kg m^{-2}) over the SYRB during 1982–2019. Their correlation coefficient is 0.73, which passes 0.01 confidence level based on Student's *t*-test. The orange (blue) dotted line represents mean summer precipitation during 1982–2002 (2003–2019). (b) Time series of water vapor content (black line; units: kg m^{-2}) and net water vapor influxes (green line; units: 10^{13} kg) over the SYRB in summer during 1982–2019. Their correlation coefficient is 0.84, which passes 0.01 confidence level based on Student's *t*-test. (For interpretation of the references to colour in this figure legend, the reader is referred to the web version of this article.)

correlated with water vapor content in the study domain ($r = 0.46$, $p < 0.01$); in the zonal direction, the net water vapor transport of the western and eastern boundaries is also significantly correlated with water vapor content in the study domain ($r = 0.54$, $p < 0.01$). Hence, the variability of water vapor transport from both meridional and zonal paths to the SYRB region is critical to summer precipitation variability. The zonal water vapor transport is generally from the west, and the meridional water vapor transport is generally from the south (Fig. 4).

The above mean water vapor flux pattern shows the approximate pathways of water vapor transport during 1982–2019, but the sources of the water vapor need to be identified and quantified. Fig. 5 provides the spatial distributions of the mean water vapor trajectory for 1 day (Fig. 5a), 5 days (Fig. 5b) and 10 days (Fig. 5c) before the air particles arrive at the SYRB during 1982–2019. The amount of water vapor trajectory is smaller the further away from the SYRB; and it decreases evenly from the middle to the sides 1 day before the water vapor arrives at the SYRB (Fig. 5a). When we retrace the trajectory for 5 days, the distributions of contribution become asymmetrical, extending mainly toward the west and south (Fig. 5b). Water vapor transport paths gradually emerge. Fig. 5c shows that water vapor can be traced westward to the Caspian Sea and Mediterranean Sea. In the southwestern and southeastern directions, it can be traced to the Bay of Bengal and Arabian Sea and to the South China Sea and the western Pacific, respectively. The large-value band in the east-west direction depicts the westerly that brings in much water vapor, and the large-value band in the northeast-southwest direction is dominated by summer monsoon.

The water vapor paths identified by the DRM are consistent with the climatological water vapor flux. So, we used the moisture source attribution method to quantify the contribution and propose the mechanism for the precipitation increase during 2003–2019 compared with 1982–2002. The moisture sources and their contributions to summer precipitable water in the SYRB are shown in Fig. 6a. The contribution pattern can distinguish how much a unit area of different sources contributed along the water vapor paths. The contribution is smaller farther away from the SYRB. The two main contribution bands obviously extend toward the west and south, and these two bands are consistent with the water vapor transport paths. The total contribution of moisture sources backward tracked over 10 days is 95.4%, including 10.6% local contribution of the SYRB and 84.8% external moisture source contribution. It shows that water vapor influxes are important for precipitation in the SYRB during 1982–2019. The remaining untracked water vapor originated 10 days ago, which only accounts for 4.6%. Because different regions have their own hydrological characteristics, the entire source region is divided into five subregions to explore the water vapor supply and relative contribution (Fig. 6a). The mean moisture contribution of each moisture source subregion during 1982–2019 is shown in Fig. 6b: the Tibetan Plateau area is 35.8%, the central Eurasian area is 22.5%, the South Asia-northern Indian Ocean area is 14.6%, the South China Sea-western Pacific area is 6.6%, and the North Africa-West Asia area is 5.3%.

As the summer precipitation in the SYRB increased significantly during 2003–2019 compared with that during 1982–2002, we calculated the change of moisture contribution in each moisture source subregion (Fig. 7). The contribution of the South Asia-northern Indian Ocean area decreased most significantly by −1.59%, and that of the Tibetan Plateau area also decreased by −0.25%. Their relative growth rates (the absolute difference of the mean moisture contribution between 1982–2002 and 2003–2019 as a percentage of that in 1982–2002) were −10.41% and −0.71%, respectively. However, the contributions of the South China Sea-western Pacific area, central Eurasian area and

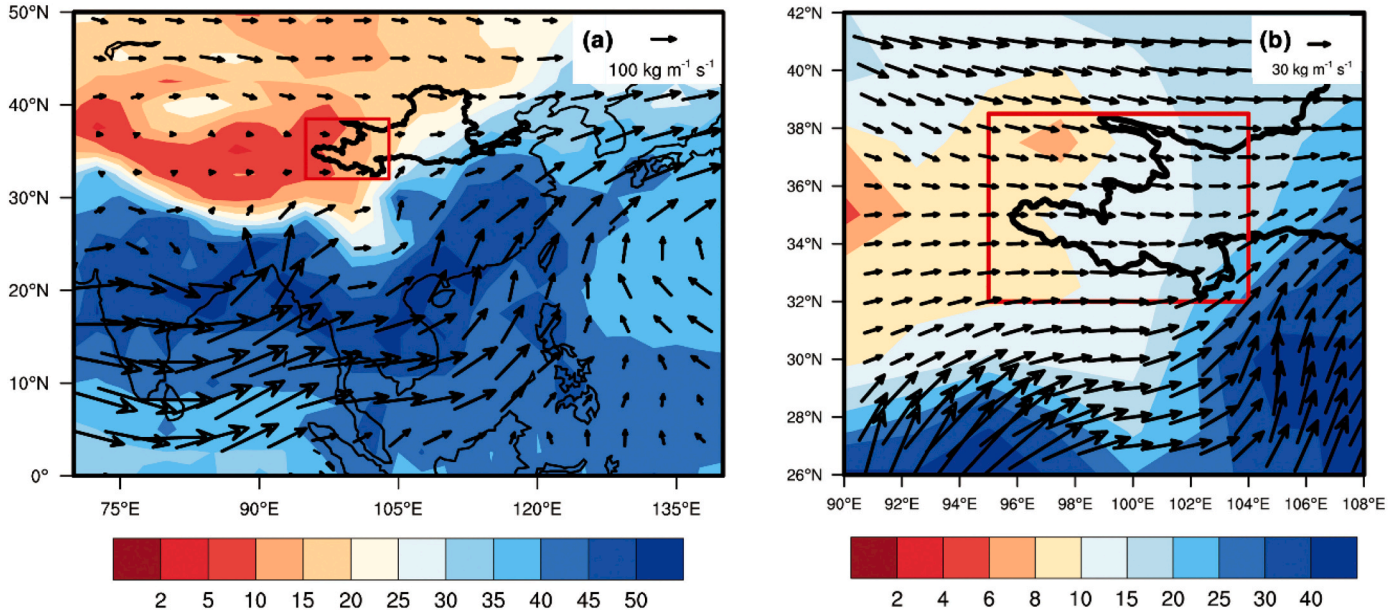

Fig. 4. (a) Spatial patterns of mean atmospheric water vapor content (shading; units: kg m^{-2}) and water vapor flux (black arrow; units: 100 kg m^{-1} s^{-1}) during 1982–2019. (b) is zoomed from panel (a) around the SYRB. The SYRB is in the red box. (For interpretation of the references to colour in this figure legend, the reader is referred to the web version of this article.)

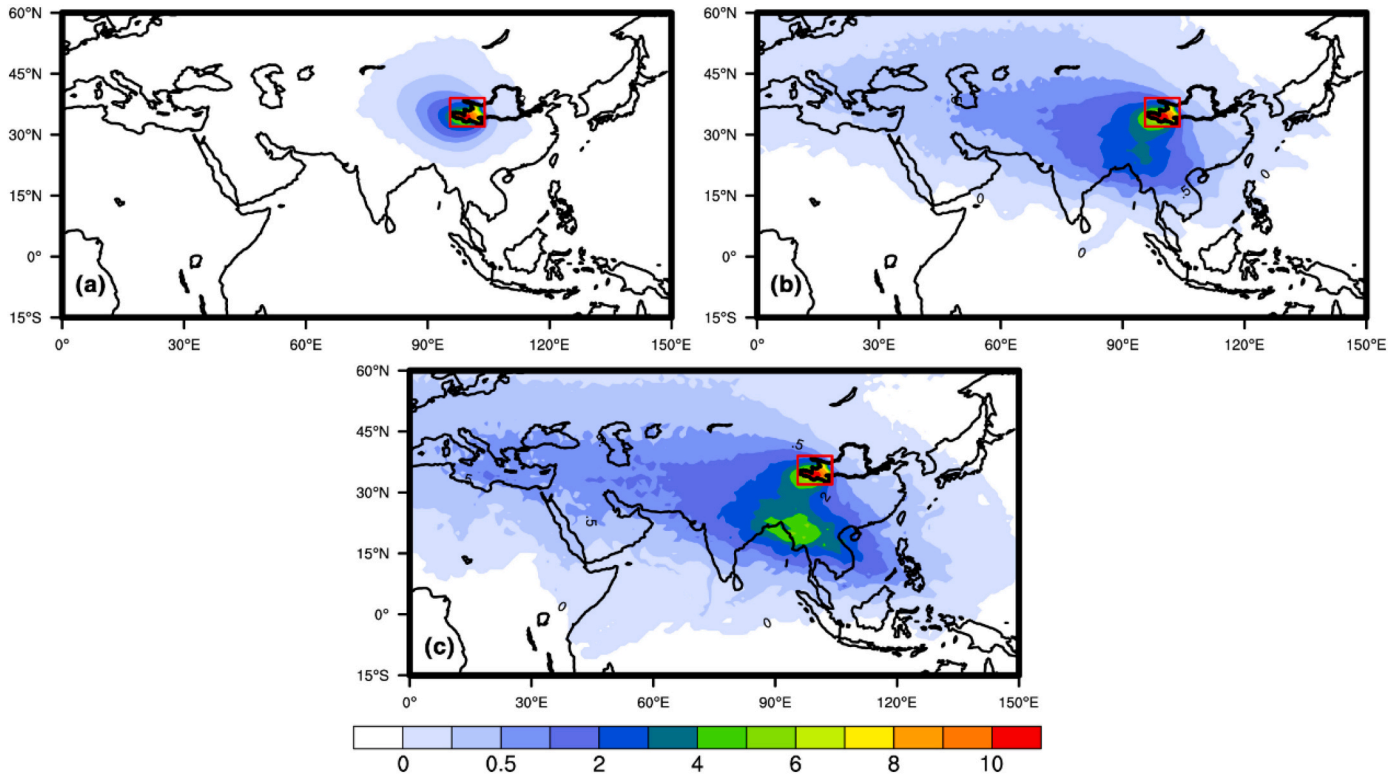

Fig. 5. Spatial distributions of the mean amount of moisture trajectory 1 day (a), 5 days (b) and 10 days (c) before the water vapor (units: 10^3 times) arrived at the SYRB during 1982–2019.

North Africa-West Asia area increased by 0.94%, 0.54% and 0.24%, respectively; their relative growth rates were 15.07%, 2.40% and 4.55%, respectively. These three subregions had larger moisture contributions to the water vapor in the SYRB during 2003–2019 compared with 1982–2002, which may explain why the precipitation in the SYRB increased during 2003–2019.

The contribution of each moisture source subregion was mainly related to the local water vapor supply amount, and the water vapor supply is dependent on evapotranspiration minus precipitation (*E*-P). The difference of E-P over each moisture source subregion is consistent with the summer precipitable water contribution ratio between the two periods (Fig. 8a). The South Asia-northern Indian Ocean area had a significant decrease (-18.27×10^4 mm a^{-1}), while the Tibetan Plateau area had a slight decrease (-0.06×10^4 mm a^{-1}); the relative growth

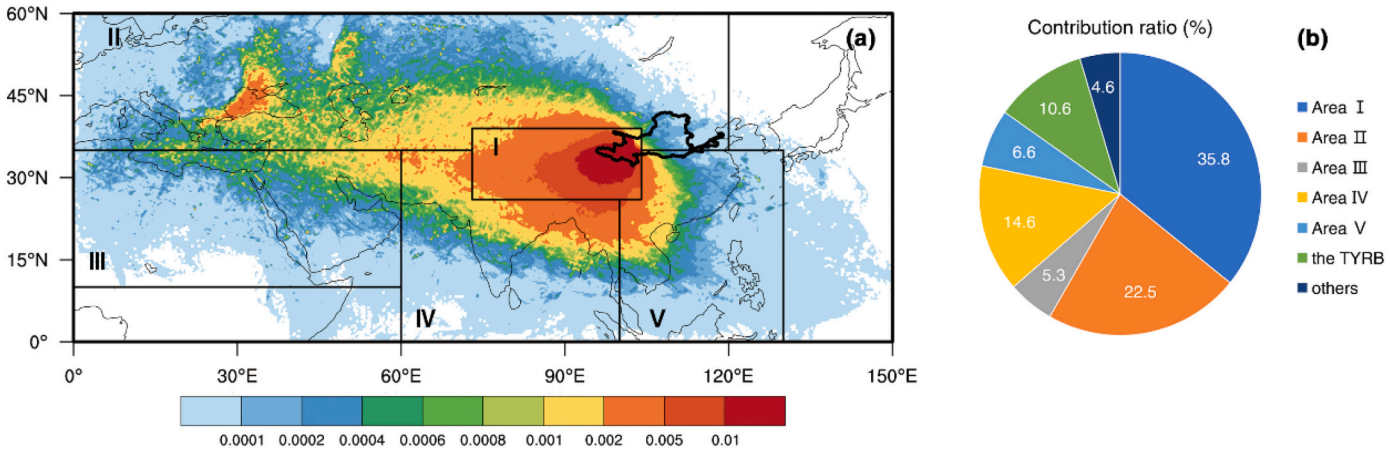

Fig. 6. (a) Spatial distribution of the mean contribution of moisture sources to the SYRB's precipitable water (units: %) during 1982–2019. Defined geographic subregions: the Tibetan Plateau area (I: 73°–104°E, 26°–39°N, except for the SYRB), central Eurasian area (II: 0°-120°E, 35°–60°N, except for part of Part I), North Africa-West Asia area (III: 0°–60°E, 10°–35°N), South Asia-northern Indian Ocean area (IV: 60°-100°E, 0°–35°N, except for part of Part I), and South China Sea-western Pacific area (V: 100°–140°E, 0°–35°N, except for part of Part I). (b) The mean moisture contribution ratio of each moisture source subregion in panel (a) to the SYRB's precipitable water (units: %) during 1982–2019.

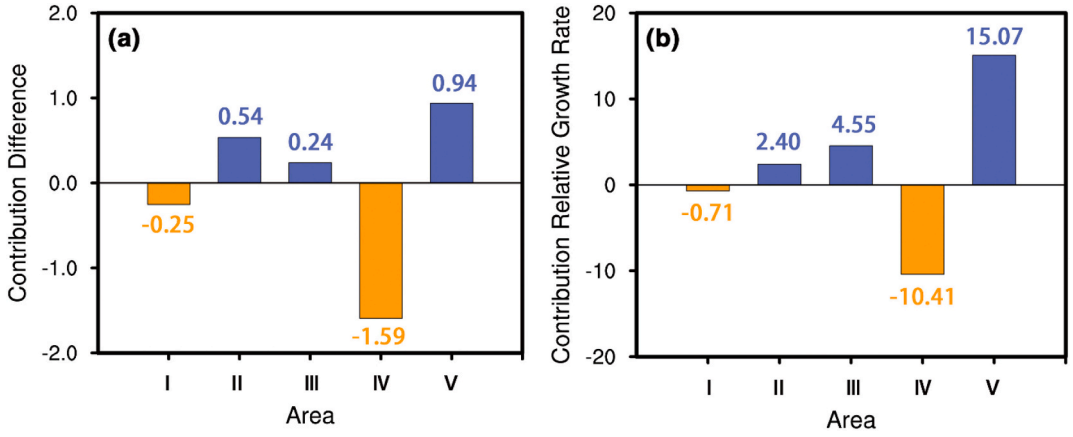

Fig. 7. (a) Difference of mean moisture contribution between 1982–2002 and 2003–2019 in each moisture source subregion. (b) The relative growth rate of moisture contribution in each moisture source subregion during 2003–2019 compared to 1982–2002. Units: %.

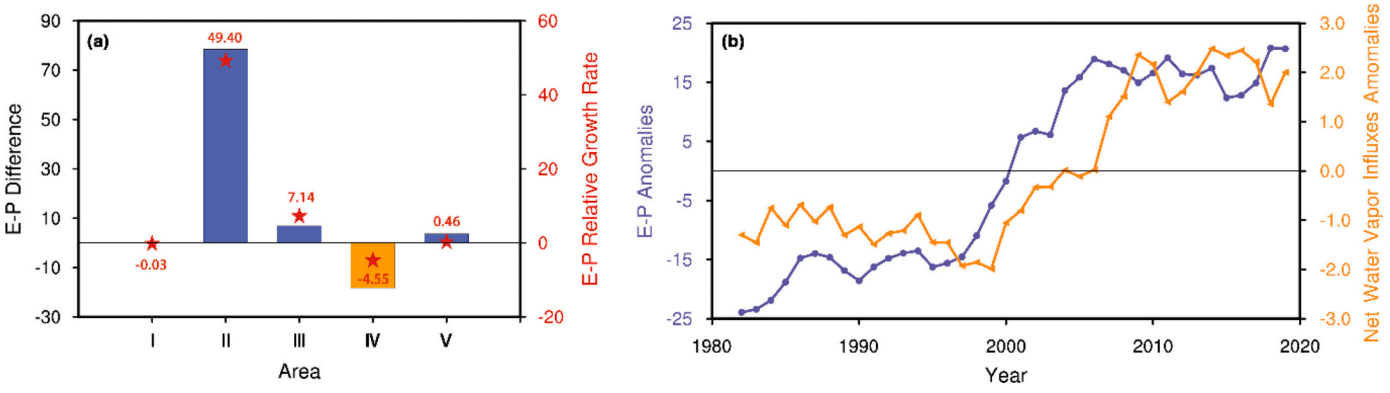

Fig. 8. (a) Difference of E-P between 1982–2002 and 2003–2019 in each moisture source subregion. Units: 10^4 mm a^{-1}. The red stars represent the relative growth rate of E-P in each moisture source subregion during 2003–2019 compared to 1982–2002. (b) Time series of E-P anomalies (blue colour; units: 10^4 mm a^{-1}) (the sum in central Eurasian area, South China Sea-western Pacific area and North Africa-West Asia area) and the net water vapor fluxes anomalies into the SYRB (orange colour; units: 10^{-13} kg a^{-1}) on 11-year moving average. (For interpretation of the references to colour in this figure legend, the reader is referred to the web version of this article.)

rates of the two subregions were − 4.55% and − 0.03%, respectively. The water vapor supplies from these two moisture sources were reduced. Obvious increase of *E*-P occurred in the central Eurasian area (78.46×10^4 mm a^{-1}), South China Sea-western Pacific area (3.66×10^4 mm a^{-1}) and North Africa-West Asia area (6.91×10^4 mm a^{-1}); the relative growth rates of these three subregions were 49.4%, 0.46% and 7.41%, respectively. This indicates the water vapor supplies from these three subregions obviously increased after 2002, which provided more water vapor to the SYRB. Under global climate change, the mainland of North Africa and the Eurasian continent tend to be drier, because more water vapor is released into the atmosphere (Byrne and O'Gorman, 2015; Routson et al., 2019). Fig. 8b shows that the sum of E-P over the three contribution-increased moisture source subregions had a significant increase after 2002, which offset and even increased the water vapor transport into the SYRB. The correlation coefficient between *E*-P and the net water vapor flux into the SYRB is 0.84 at the 0.01 confidence level on the decadal scale. Therefore, the water vapor transports from these three moisture source subregions increased, causing the precipitation increase over the SYRB during 2003–2019.

4. Conclusions and discussion

The summer precipitation in the SYRB increased by approximately 11.4% during 2003–2019 compared with that during 1982–2002. It was mainly influenced by water vapor influxes during 1982–2019, which was traced westward to the Caspian Sea and Mediterranean Sea, and southward to the Bay of Bengal, Arabian Sea, South China Sea, and western Pacific by the DRM. During 1982–2019, the mean moisture contribution ratios of the Tibetan Plateau area, central Eurasian area, South Asia-northern Indian Ocean area, South China Sea-western Pacific area, and North Africa-West Asia area to the summer precipitable water in the SYRB were 35.8%, 22.5%, 14.6%, 6.6%, and 5.3%, respectively. Compared with the 1982–2002 period, the relative growth rates of moisture contribution from the central Eurasian area, North Africa-West Asia area and South China Sea-western Pacific area were increased by 15.07%, 4.55% and 2.40% during 2003–2019. These three subregions were the main moisture sources for the precipitation increase after 2002. Furthermore, the interdecadal change in E-P was consistent with the moisture contribution, which provided sufficient water vapor to the SYRB for the summer precipitation increase during 2003–2019. Accordingly, the water vapor from the three contribution-increased moisture source subregions offset other sources' moisture supply reduction and even led to an overall increase in water vapor during 2003–2019 compared with 1982–2002, resulting in a noteworthy increase in summer precipitation in the SYRB during 2003–2019.

Our study illustrates the changes in water resources in the SYRB, providing guidance for regional water resources utilization and ecological protection. However, some issues need to be considered. Under global warming, the global water cycle accelerated and regional water resources changed (Sun et al., 2007). The water vapor transport is the indispensable part of the water cycle, which can be separated into stationary and transient components (Trenberth, 1991). Since the stationary component is dominant in the total water vapor transport (Feng and Zhou, 2012; Simmonds et al., 1999), the transient component is usually ignored on the long-time scales. As the demand for accuracy increases, more attention should be paid to the transient component. In addition, the simple DRM is well fitted to study large-scale climatological moisture sources, because it is flexible in the type of input data and computationally efficient (Dominguez et al., 2020). However, the two-dimensional DRM ignores vertical movement, which would incorrectly estimate some details of water vapor transport processes. Whether these deviations can be ignored depends on the time scales and areas studied. In the context of global climate change, more detailed and shorter time scales of regional hydrological cycles must be investigated urgently. It remains a challenge to fully understand the hydrological cycle in the YRB, especially its physical mechanisms.

Data availability statement

The Global Precipitation Climatology Centre (GPCC) data are available for download (https://www.dwd.de/EN/ourservices/gpcc/gpcc.html). The National Center for Environmental Prediction/National Center for Atmospheric Research (NCEP/NCAR) reanalysis data are download from https://psl.noaa.gov/data/gridded/data.ncep.reanalysis.html. The European Centre for Medium-Range Weather Forecasts reanalysis (ERA5) data are derived from https://cds.climate.copernicus.eu/cdsapp#!/dataset/reanalysis-era5-pressure-levels?tab=overview and https://cds.climate.copernicus.eu/cdsapp#!/dataset/reanalysis-era5-single-levels-monthly-means?tab=overview.

Declaration of Competing Interest

The authors declare that they have no known competing financial interests or personal relationships that could have appeared to influence the work reported in this paper.

Acknowledgments

This work is supported by the National Science Foundation of China (42041004 and 41991231), the Strategic Priority Research Program of the Chinese Academy of Sciences (Grant No. XDA2006010301), and the central universities (lzujbky-2019-kb30). The authors thank the Global Precipitation Climatology Centre, the National Center for Environmental Prediction/National Center for Atmospheric Research and the European Centre for Medium-Range Weather Forecasts reanalysis for providing accessible and excellent datasets that made this study possible. The authors also thank colleagues and other contributors.

References

Bisselink, B., Dolman, A.J., 2008. Precipitation recycling: Moisture sources over Europe using ERA-40 data. J. Hydrometeorol. 9 (5), 1073–1083. https://doi.org/10.1175/2008JHM962.1.

Byrne, M.P., O'Gorman, P.A., 2015. The response of precipitation minus evapotranspiration to climate warming: why the "wet-get-wetter, dry-get-drier" scaling does not hold over land. J. Clim. 28 (20), 8078–8092. https://doi.org/10.1175/JCLI-D-15-0369.1.

Camberlin, P., 1997. Rainfall anomalies in the source region of the Nile and their connection with the Indian summer monsoon. J. Clim. 10 (6), 1380–1392. https://doi.org/10.1175/15200442(1997)010<1380:RAITSR>2.0.CO;2.

Dominguez, F., Kumar, P., Liang, X.Z., Ting, M., 2006. Impact of atmospheric moisture storage on precipitation recycling. J. Clim. 19 (8), 1513–1530. https://journals.ametsoc.org/search?f_0=author&q_0=Praveen+Kumar.

Dominguez, F., Hu, H., Martinez, J.A., 2020. Two-layer dynamic recycling model (2L-DRM): learning from moisture tracking models of different complexity. J. Hydrometeorol. 21 (1), 3–16. https://doi.org/10.1175/JHM-D-19-0101.1.

Feng, L., Zhou, T., 2012. Water vapor transport for summer precipitation over the Tibetan Plateau: Multidata set analysis. J. Geophys. Res. Atmos. 117 (D20) https://doi.org/10.1029/2011JD017012.

Feng, J., Wang, T., Xie, C., 2006. Eco-environmental degradation in the source region of the Yellow River, Northeast Qinghai-Xizang Plateau. Environ. Monit. Assess. 122 (1), 125–143. https://doi.org/10.1007/s10661-005-9169-2.

Gao, G., Ma, Y., Fu, B., 2016. Multi-temporal scale changes of streamflow and sediment load in a loess hilly watershed of China. Hydrol. Process. 30 (3), 365–382. https://doi.org/10.1002/hyp.10585.

Guan, X., Zhu, K., Huang, X., Zeng, X., He, Y., 2021. Precipitation changes in semi-arid regions in East Asia under global warming. Front. Earth Sci. 9, 1030. https://doi.org/10.3389/feart.2021.762348.

Hassan, M.A., Church, M., Xu, J., Yan, Y., 2008. Spatial and temporal variation of sediment yield in the landscape: example of Huanghe (Yellow River). Geophys. Res. Lett. 35 (6) https://doi.org/10.1029/2008GL033428.

He, Y., Tian, W., Huang, J., Wang, G., Ren, Y., Yan, H., Yu, H., Guan, X., Hu, H., 2021. The mechanism of increasing summer water vapor over the Tibetan Plateau. J. Geophys. Res. Atmos. 126 https://doi.org/10.1029/2020JD034166 e2020JD034166.

Hu, Y., Maskey, S., Uhlenbrook, S., Zhao, H., 2011. Streamflow trends and climate linkages in the source region of the Yellow River, China. Hydrol. Process. 25 (22), 3399–3411. https://doi.org/10.1002/hyp.8069.

Hua, L., Zhong, L., Ke, Z., 2017. Characteristics of the precipitation recycling ratio and its relationship with regional precipitation in China. Theor. Appl. Climatol. 127 (3), 513–531. https://doi.org/10.1007/s00704-015-1645-1.

Huang, W., Feng, S., Chen, J., Chen, F., 2015. Physical mechanisms of summer precipitation variations in the Tarim Basin in northwestern China. J. Clim. 28 (9), 3579–3591. https://doi.org/10.1175/JCLI-D-14-00395.1.
Huang, J., Zhang, G., Yu, H., Wang, S., Guan, X., Ren, Y., 2020. Characteristics of climate change in the Yellow River basin during recent 40 years (in Chinese). J. Hydraul. Eng. 51 (9), 1048–1058. https://doi.org/10.13243/j.cnki.slxb.20200603.
Jiang, P., Yu, Z., Yuan, F., Acharya, K., 2019. The multi-scale temporal variability of extreme precipitation in the source region of the Yellow River. Water 11 (1), 92. https://doi.org/10.3390/w11010092.
Kalnay, E., Kanamitsu, M., Kistler, R., Collins, W., Deaven, D., Gandin, L., Iredell, M., Saha, S., White, G., Woollen, J., Zhu, Y., Chelliah, M., Ebisuzaki, W., Higgins, W., Janowiak, J., Mo, K.C., Ropelewski, C., Wang, J., Leetmaa, A., Reynolds, R., Jenne, R., Joseph, D., 1996. The NCEP/NCAR 40-year reanalysis project. Bull. Am. Meteorol. Soc. 77 (3), 437–471. https://doi.org/10.1175/1520-0477(1996)077<0437:TNYRP>2.0.CO;2.
Lan, Y., Zhao, G., Zhang, Y., Wen, J., Liu, J., Hu, X., 2010. Response of runoff in the source region of the Yellow River to climate warming. Quat. Int. 226 (1–2), 60–65. https://doi.org/10.1016/j.quaint.2010.03.006.
Li, Q., Yang, M., Wan, G., Wang, X., 2016. Spatial and temporal precipitation variability in the source region of the Yellow River. Environ. Earth Sci. 75 (7), 594. https://doi.org/10.1007/s12665-016-5583-8.
Li, J., Xie, S.P., Cook, E.R., Chen, F., Shi, J., Zhang, D.D., Fang, K., Gou, X., Li, T., Peng, J., Shi, S., Zhao, Y., 2019. Deciphering human contributions to Yellow River flow reductions and downstream drying using centuries-long tree ring records. Geophys. Res. Lett. 46 (2), 898–905. https://doi.org/10.1029/2018GL081090.
Liang, S., Ge, S., Wan, L., Zhang, J., 2010. Can climate change cause the Yellow River to dry up? Water Resour. Res. 46 (2), W02505. https://doi.org/10.1029/2009WR007971.
Lin, A.M., Yang, Z.Y., Sun, Z.M., Yang, T.S., 2001. How and when did the Yellow River develop its square bend? Geology 29 (10), 951–954. https://doi.org/10.1130/0091-7613(2001)029<0951:HAWDTY>2.0.CO;2.
Lin, P., Pan, M., Beck, H.E., Yang, Y., Yamazaki, D., Frasson, R., David, C.H., Durand, M., Pavelsky, T., Allen, G., Gleason, C., Wood, E.F., 2018. Spatiotemporal evaluation of simulated evapotranspiration and streamflow over Texas using the WRF-Hydro-RAPID modeling framework. JAWRA J. Am. Water Resour. Assoc. 54 (1), 40–54. https://doi.org/10.1111/1752-1688.12585.
Ma, Y., Lu, M., Chen, H., Pan, M., Hong, Y., 2018. Atmospheric moisture transport versus precipitation across the Tibetan Plateau: a mini-review and current challenges. Atmos. Res. 209, 50–58. https://doi.org/10.1016/j.atmosres.2018.03.015.
Mrudula, G., 2016. Water vapor transport from the Indian monsoon region: the phenomenon of Atmospheric River. Remote Sensing and Modeling of the Atmosphere, Oceans, and Interactions VI. Int. Soc. Optics Photon. 9882, 98821S. https://doi.org/10.1117/12.2223666.
Peng, D., Zhou, T., Zhang, L., 2020. Moisture sources associated with precipitation during dry and wet seasons over Central Asia. J. Clim. 33 (24), 10755–10771. https://doi.org/10.1175/JCLI-D-20-0029.1.
Ren, Y., Yu, H., Liu, C., He, Y., Huang, J., Zhang, L., Hu, H., Zhang, Q., Chen, S., Liu, X., Zhang, M., Wei, Y., Yan, Y., Fan, W., Zhou, J., 2021. Attribution of dry and wet climatic changes over Central Asia. J. Clim. 1-57 https://doi.org/10.1175/JCLI-D-21-0329.1.
Routson, C.C., McKay, N.P., Kaufman, D.S., Erb, M.P., Goosse, H., Shuman, B.N., Rodysill, J.R., Ault, T., 2019. Mid-latitude net precipitation decreased with Arctic warming during the Holocene. Nature 568 (7750), 83–87. https://doi.org/10.1038/s41586-019-1060-3.
Schneider, U., Becker, A., Finger, P., Meyer-Christoffer, A., Ziese, M., Rudolf, B., 2014. GPCC's new land surface precipitation climatology based on quality-controlled in situ data and its role in quantifying the global water cycle. Theor. Appl. Climatol. 115 (1–2), 15–40. https://doi.org/10.1007/s00704-013-0860-x.
Simmonds, I., Bi, D., Hope, P., 1999. Atmospheric water vapor flux and its association with rainfall over China in summer. J. Clim. 12 (5), 1353–1367. https://doi.org/10.1175/1520-0442(1999)012<1353:AWVFAI>2.0.CO;2.
Sodemann, H., Schwierz, C., Wernli, H., 2008. Interannual variability of Greenland winter precipitation sources: Lagrangian moisture diagnostic and North Atlantic Oscillation influence. J. Geophys. Res. Atmos. 113 (D3), 2008. https://doi.org/10.1029/2007JD008503.
Stohl, A., James, P., 2004. A Lagrangian analysis of the atmospheric branch of the global water cycle. Part I: Method description, validation, and demonstration for the August 2002 flooding in central Europe. J. Hydrometeorol. 5 (4), 656–678. https://doi.org/10.1175/1525-7541(2004)005%3C0656:ALAOTA%3E2.0.CO;2.
Sun, Y., Solomon, S., Dai, A., Portmann, R.W., 2007. How often will it rain? J. Clim. 20 (19), 4801–4818. https://doi.org/10.1175/JCLI4263.1.
Sun, B., Zhu, Y., Wang, H., 2011. The recent interdecadal and interannual variation of water vapor transport over eastern China. Adv. Atmos. Sci. 28 (5), 1039–1048. https://doi.org/10.1007/s00376-010-0093-1.
Trenberth, K.E., 1991. Climate diagnostics from global analysis: conservation of mass in ECMWF analysis. J. Clim. 4 (7), 707–722. https://doi.org/10.1175/1520-0442(1991)004<0707:CDFGAC>2.0.CO;2.
Trenberth, K.E., Dai, A., Rasmussen, R.M., Parsons, D.B., 2010. The changing character of precipitation. Bull. Am. Meteorol. Soc. 84 (9), 1205–1218. https://doi.org/10.1175/BAMS-84-9-1205.
Wang, H., Chen, H., 2012. Climate control for southeastern China moisture and precipitation: Indian or East Asian monsoon? J. Geophys. Res. Atmos. 117, D12109. https://doi.org/10.1029/2012JD017734.
Wang, G., Qian, J., Cheng, G., Lai, Y., 2001. Eco-environmental degradation and causal analysis in the source region of the Yellow River. Environ. Earth Sci. 40 (7), 884–890. https://doi.org/10.1007/s002540100248.
Wang, H., Yang, Z., Saito, Y., Liu, J.P., Sun, X., 2006. Interannual and seasonal variation of the Huanghe (Yellow River) water discharge over the past 50years: connections to impacts from ENSO events and dams. Glob. Planet. Chang. 50 (3–4), 212–225. https://doi.org/10.1016/j.gloplacha.2006.01.005.
Wang, X., Chen, D., Pang, G., Gou, X., Yang, M., 2021. Historical and future climates over the upper and middle reaches of the Yellow River Basin simulated by a regional climate model in CORDEX. Clim. Dyn. 56 (9–10), 2749–2771. https://doi.org/10.1007/s00382-020-05617-4.
Wu, Y., Yang, S., Hu, X., Wei, W., 2020. Process-based attribution of long-term surface warming over the Tibetan Plateau. Int. J. Climatol. 40 (15), 6410–6422. https://doi.org/10.1002/joc.6589.
Yao, J., Liu, H., Huang, J., Gao, Z., Wang, G., Li, D., Yu, H., Chen, X., 2020. Accelerated dryland expansion regulates future variability in dryland gross primary production. Nat. Commun. 11 (1), 1–10. https://doi.org/10.1038/s41467-020-15515-2.
Yuan, F., Berndtsson, R., Zhang, L., Uvo, C.B., Hao, Z., Wang, X., Yasuda, H., 2015. Hydro climatic trend and periodicity for the source region of the Yellow River. J. Hydrol. Eng. 20 (10), 05015003. https://doi.org/10.1061/(ASCE)HE.1943-5584.0001182.
Yuan, F., Yasuda, H., Berndtsson, R., Bertacchi Uvo, C., Zhang, L., Hao, Z., Wang, X., 2016. Regional Sea-surface temperatures explain spatial and temporal variation of summer precipitation in the source region of the Yellow River. Hydrol. Sci. J. 61 (8), 1383–1394. https://doi.org/10.1080/02626667.2015.1035658.
Yuan, F., Liu, J., Berndtsson, R., Hao, Z., Cao, Q., Wang, H., Du, Y., An, D., 2020. Changes in Precipitation extremes over the source region of the yellow river and its relationship with teleconnection patterns. Water 12 (4), 978. https://doi.org/10.3390/w12040978.
Zhang, R., 2001. Relations of water vapor transport from Indian monsoon with that over East Asia and the summer rainfall in China. Adv. Atmos. Sci. 18 (5), 1005–1017. https://doi.org/10.1007/BF03403519.
Zhang, Y., Su, F., Hao, Z., Xu, C., Yu, Z., Wang, L., Tong, K., 2015. Impact of projected climate change on the hydrology in the headwaters of the Yellow River basin. Hydrol. Process. 29 (20), 4379–4397. https://doi.org/10.1002/hyp.10497.
Zhao, Y., Zhou, T., Li, P., Furtado, K., Zou, L., 2021. Added value of a convection permitting model in simulating atmospheric water cycle over the Asian Water Tower. J. Geophys. Res. Atmos. 126 (13) https://doi.org/10.1029/2021JD034788 e2021JD034788.
Zhu, K., Guan, X., Huang, J., Wang, J., Guo, S., Cao, C., 2021. Precipitation over semi-arid regions of North Hemisphere affected by Atlantic Multidecadal Oscillation. Atmos. Res. 262, 105801 https://doi.org/10.1016/j.atmosres.2021.105801.